Beam-Normal Single-Spin Asymmetry in ^{208}Pb at Low Energy: Discrepancy Resolved or New Kinematic Puzzle?

A. Esser[1], N. Kozyrev[1], K. Aulenbacher[1,2,3], S. Baunack[1], M. Dehn[1], A. Del Vincio,[1,4]
L. Doria[1], M. Hoek[1], F. Keil[1], F. Maas[1,2,3], H. Merkel,[1,3] M. Mihovilovič[5,6], U. Müller[1], J. Pochodzalla,[1,2]
B. S. Schlimme,[1] T. Shao[1], S. Stengel[1], M. Thiel[1], L. Wilhelm[1], and C. Sfienti[1,2,3]

[1]*Institut für Kernphysik, Johannes Gutenberg-Universität Mainz, D-55099 Mainz, Germany*
[2]*Helmholtz Institute Mainz, GSI Helmholtzzentrum für Schwerionenforschung, Darmstadt, Johannes Gutenberg-Universität,
D-55099 Mainz, Germany*
[3]*PRISMA$^+$ Cluster of Excellence, Johannes Gutenberg-Universität, D-55099 Mainz, Germany*
[4]*Dipartimento di Fisica "E. Fermi," Universitá di Pisa, Pisa, Italy*
[5]*Jožef Stefan Institute, SI-1000 Ljubljana, Slovenia*
[6]*Faculty of Mathematics and Physics, University of Ljubljana, SI-1000, Ljubljana, Slovenia*

A long-standing discrepancy between measured and predicted beam-normal single-spin asymmetries A_n in elastic electron scattering off ^{208}Pb has challenged our understanding of two-photon exchange (TPE) in heavy nuclei. We report a new measurement at 570 MeV and $Q^2 = 0.04 \text{ GeV}^2/c^2$, yielding $A_n = [-9.1 \pm 2.1(\text{stat}) \pm 0.7(\text{syst})]$ ppm. This nonzero value contrasts with previous results at higher energies and suggests a kinematic dependence of TPE effects not captured by current theory, prompting a reevaluation of earlier interpretations.

Understanding the fundamental dynamics of electron scattering is essential for precision tests of the Standard Model, the determination of nucleon and nuclear structure, and the interpretation of a wide range of experimental observables. While the leading-order one-photon exchange approximation provides a successful description of most processes, higher-order contributions—particularly those arising from two-photon exchange (TPE)—have emerged as a critical source of theoretical uncertainty [1,2]. TPE processes, in which the electron interacts via the exchange of two virtual photons with the target, encode essential information about hadronic structure and dynamics that is not accessible at leading order. They have been invoked to explain long-standing discrepancies in the extraction of proton electromagnetic form factors [3], contribute to theoretical uncertainties in parity-violating electron scattering (PVES)—where TPE enters alongside dominant γ-Z box corrections [4], and crucially enter the interpretation of muonic atom spectroscopy [5]—where they currently limit the precision with which nuclear charge radii can be determined. Despite their relatively small size, typically at the percent level, TPE effects become decisive whenever

experiments push the limits of precision. A rare opportunity to isolate TPE effects is offered by the beam-normal single-spin asymmetry A_n. This asymmetry arises in elastic electron scattering when the incident beam is polarized normal to the scattering plane (often referred to as beam-normal polarization). It is defined as

$$A_n = \frac{\sigma^\uparrow - \sigma^\downarrow}{\sigma^\uparrow + \sigma^\downarrow}, \qquad (1)$$

where $\sigma^\uparrow$ and $\sigma^\downarrow$ are the cross sections for spin parallel and antiparallel to the normal vector $\hat{n} = (\vec{k} \times \vec{k}')/|\vec{k} \times \vec{k}'|$ of the scattering plane, with $\vec{k}$ and $\vec{k}'$ the three-momenta of the incoming and scattered electrons, respectively.

At leading order A_n arises from the imaginary (absorptive) part of the interference between the one- and two-photon exchange amplitudes [6]. Several theoretical approaches have been developed to calculate A_n in electron scattering. For the $p(e, e')p$ reaction, multiple methods are available [7,8]. However, for nuclear targets with $Z \geq 2$, only two established models exist. The Coulomb-distorted wave approach [9] includes all orders of photon exchange but only the nuclear ground state. The dispersion relation framework [10] incorporates excited intermediate states but is valid only at low momentum transfer and introduces uncertainty through the poorly constrained Compton form factor. In both cases, predictions for heavy nuclei rely on extrapolations and assumptions whose validity is limited to

specific energy and momentum-transfer ranges. This limitation became evident with the unexpected result from the HAPPEX and PREX Collaborations [11], which reported $A_n = 0.28 \pm 0.21_{\text{stat}} \pm 0.14_{\text{syst}}$ ppm in ^{208}Pb at $E = 1.063$ GeV and $Q^2 \sim 0.009$ GeV^2/c^2, in clear disagreement with theoretical expectations. The discrepancy was later confirmed at similar kinematics by the PREX-II/CREX measurements [12], but remains unexplained.

Motivated by this anomaly, a measurement program using the A1 high-resolution spectrometers [13] at MAMI [14] was launched to study A_n across different nuclear targets [15,16]. Results for ^{12}C, ^{28}Si, and ^{90}Zr were generally consistent with the dispersion-based prediction within its estimated 20% uncertainty. No dramatic suppression of A_n—like that seen in ^{208}Pb—was observed. In this Letter, we present the first measurement of A_n in elastic electron scattering from ^{208}Pb at $E = 570$ MeV and $Q^2 = 0.04$ GeV^2/c^2. The kinematics match earlier measurements on lighter nuclei, enabling a direct comparison and testing the nuclear and kinematic dependence of TPE.

To measure A_n a vertically polarized continuous-wave electron beam with an energy of 570 MeV was scattered from a ^{208}Pb foil of 0.5 mm thickness (567 mg cm^{-2}), corresponding to about one-tenth of a radiation length. This thickness optimized the reaction rate while minimizing depolarization from multiple scattering and target damage. The foil was mounted in a copper frame connected to a heat exchanger cooled to 5 °C. Fast steering magnets rastered the beam over an area of approximately 4×4 mm^2 to reduce local heating; the raster signals were synchronized with the readout gates to suppress false asymmetries from thickness variations.

Two magnetic spectrometers (A and B) were positioned symmetrically around the beam pipe at forward angles, defining a momentum transfer of $Q^2 = 0.04$ GeV^2/c^2, matching earlier measurements on lighter nuclei. At this Q^2, the elastic cross section for ^{208}Pb shows a local minimum, resulting in lower rates than in previous measurements on ^{12}C and ^{28}Si [15,16]. Elastically scattered electrons were detected in fused-silica Čerenkov detectors placed in the focal planes of the high-resolution spectrometers, read out by UV-sensitive photo multiplier tubes (PMT). Each detector consisted of multiple PMTs optically coupled to the radiator bars. Initial alignment and calibration data were taken at low current (50 nA) with tracking detectors, which were then switched off during physics runs at 20 μA to prevent damage.

A key component of this experiment was the newly developed data acquisition system, described in detail in Ref. [17]. Specifically designed for high-precision asymmetry measurements at low rates, it employed four modular field-programmable gate array (FPGA) boards to count individual PMT pulses instead of integrating a current, thereby reducing statistical uncertainty. A master FPGA synchronized readout gates to the 50 Hz power-grid frequency and generated pseudorandom sequences of beam-polarity states using de Bruijn patterns [18], which ensure that all possible polarity combinations occur with equal frequency and thus effectively suppress polarity-correlated systematics. PMT signals were processed using NINO discriminators [19] with channel-specific attenuation, and threshold settings which were optimized through dedicated scans based on pulse-height spectra.

Beam diagnostics were integrated via voltage-to-frequency converters located close to the monitors, enabling high-resolution digitization of current, position, and energy. This minimized analog noise and allowed event-by-event asymmetry corrections.

Beam polarization was measured at the start of each experimental campaign using a Møller polarimeter, cross-calibrated against a Mott system at low energy [20], providing continuous tracking of the degree and orientation of polarization. The average beam polarization was $P = (81.4 \pm 1.6)\%$. Two separated experimental campaigns (November 2023 and June 2024) allowed for stringent cross-checks of systematics; in total, 232.7 h of data were collected on the ^{208}Pb target.

The analysis was conducted using a systematic multistep procedure. It begins by excluding short periods in which the accelerator or beam stabilization systems were not functioning properly—such as during sudden beam losses or magnetic steering failures. This manual selection was deliberately conservative to preserve as much of the dataset as possible; overall only 2.8% of the events were rejected at this stage. Next, the beam monitor signals were calibrated to relate the raw electronic outputs to physical quantities. For the beam position and energy monitors, absolute calibration is not strictly necessary for the extraction of the asymmetry, as the units cancel out in the regression-based correction. Nonetheless, calibrated values are important to quantify the scale of beam fluctuations and provide physical context. To calibrate the position monitors, the electron beam was slowly rastered across two targets consisting of three thin either vertical or horizontal carbon rods with diameters of 0.5 mm. They have been mounted with a known pitch of 1.0 mm. The position of the rods was inferred from the Čerenkov detector response, allowing the beam monitor scale to be determined separately in both horizontal and vertical directions. The beam energy monitor, which already has a known transfer function, was verified by superimposing a defined voltage offset corresponding to a known energy shift. In contrast to the position and energy monitors, offsets in the beam current monitors and in the photomultiplier count rates directly impact the extracted asymmetry and therefore required precise determination. For this purpose, an automated calibration run was executed every 3 h. During these runs, the beam current was ramped up in discrete steps from 17.5 to 21.5 μA, while all detector signals were recorded. The current monitor signals were linearly fitted against the

reference from a calibrated flux gate current probe, and the PMT count offsets were extracted from linear fits of count rate versus beam current.

Following the calibrations, individual events were subjected to quality cuts. While long periods of instability had already been excluded manually, event-by-event fluctuations required an automated approach. A set of cut rules was defined to reject events with anomalous beam parameters or detector responses. The robustness of the final asymmetry against the strength of these cuts was tested by applying a range of thresholds, as illustrated in Fig. 1. The orange trumpet shape indicates the expected statistical spread of the mean under different cut strengths. To further ensure the robustness of the final analysis, the data were independently processed using two separate analysis chains, yielding consistent results (red diamonds). After data selection, the experimental asymmetry A_{expt} was obtained from detector count differences for each polarity pair, while beam and monitor parameters were stored on an event-by-event basis. This asymmetry includes contributions from helicity-correlated beam fluctuations and must be corrected to extract the physical beam-normal single-spin asymmetry. The correction was implemented via a multiparameter linear regression of the form:

$$A_n = \frac{1}{P_\perp} \cdot \Big(A_{\mathrm{expt}} - c_I A_I - c_X \Delta X - c_Y \Delta Y$$
$$- c_{X'} \Delta X' - c_{Y'} \Delta Y' - c_E \Delta E \Big),$$

where $P_\perp$ is the degree of vertical beam polarization, and the coefficients c_i represent the sensitivity of the asymmetry to helicity-correlated differences in beam current A_I, horizontal and vertical position ΔX, ΔY, angle $\Delta X'$, $\Delta Y'$, and energy ΔE. The coefficients were obtained from a simultaneous fit to the full dataset, minimizing correlations

between A_{expt} and the various beam parameters. In this way, all instrumental asymmetries were removed event by event before applying the polarization normalization.

Finally, to combine the asymmetries from different photomultiplier channels, a weighted average was computed for each spectrometer. The weighting was based on the total number of counts recorded by each channel, ensuring that channels with higher statistical power contributed proportionally more to the final value. Because of the optical coupling of the PMTs and the adjusted discriminator thresholds, the channel-to-channel variations in weight were modest. In spectrometer A, the weights varied between 0.856 and 1.105, while in spectrometer B the variation was even smaller, ranging from 0.996 to 1.003. This reflects differences in detector geometry: spectrometer B focuses elastically scattered electrons onto a compact spot, whereas spectrometer A focuses onto an extended line, leading to a slightly broader distribution of channel contributions. The final asymmetries are shown in Fig. 2, including individual PMT asymmetries and the weighted averages for each spectrometer. The combination of the two spectrometers was performed using a standard error-weighted average.

The results for A_n obtained as the arithmetic mean of the two independent analysis chains together with their uncertainties are shown in Table I. The systematic uncertainty was evaluated by varying key analysis parameters and quantifying their effect on the extracted asymmetry, following the same strategy as in our previous measurements on lighter nuclei [15,16]. The contributions from fluctuations of the beam position, angle, and energy were estimated by
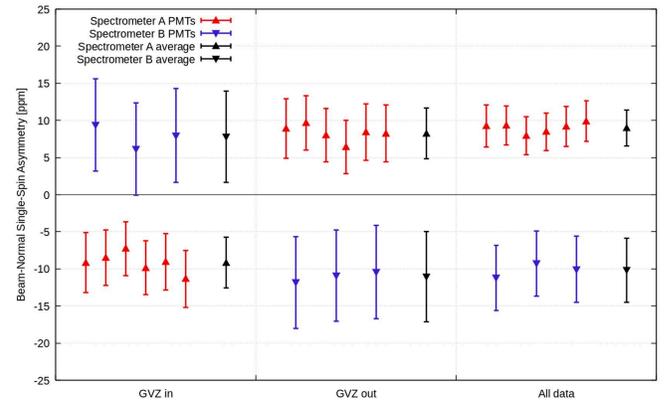
FIG. 2. Measured beam-normal single-spin asymmetry for both signs of the general polarity convention (GVZ in and GVZ out), which correspond to reversing the overall polarity sign by inserting or removing a half-wave plate in the polarized-electron source, and for the full dataset. The general sign was reversed by inserting an additional $\lambda/2$ wave plate into the laser beam of the polarized-electron source. Colored points represent individual PMTs; the black markers denote the weighted average per spectrometer. The asymmetry for spectrometer A for the full dataset has been inverted.
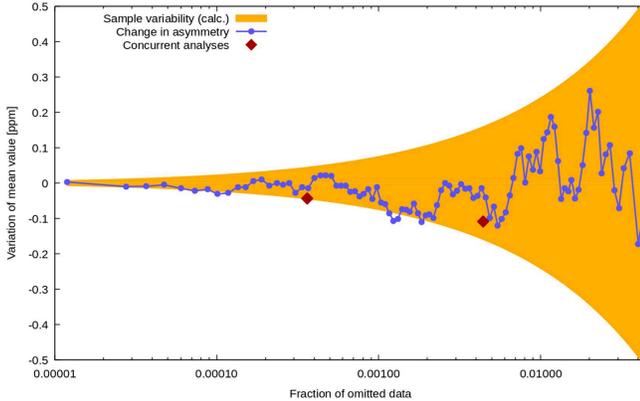

FIG. 1. Change of the measured asymmetry versus the fraction of dismissed data, for spectrometer A. The orange trumpet shape shows the expected sample variability of the mean. Blue points represent a sequence of cuts of increasing strictness. The two red diamonds indicate the values obtained by the two analysis chains.

TABLE I. Measured beam-normal single-spin asymmetries for each spectrometer. The difference in scattering angle at similar Q^2 arises from the broader angular acceptance of spectrometer A. Uncertainties are in parts per million (ppm), with statistical and systematic contributions listed separately. The first five entries correspond to asymmetry correction errors. Further contributions: ΔA_I estimates the residual beam-current asymmetry, Δ Gain assesses PMT gain variations, Δ Tails estimates for nonlinearities from large corrections, Δ Inversion accounts for the different number of events in both states of the half-wave plate, Δ Analysis quantifies the spread between the two independent analysis chains, and ΔP gives the polarization uncertainty.

Spectrometer	A	B
Scattering angle	20.14°	20.56°
Q^2 (GeV$^2/c^2$)	0.040	0.041
A_n (ppm)	8.954	9.568
$\Delta(\partial\sigma/\partial x)$	< 0.001	< 0.001
$\Delta(\partial\sigma/\partial y)$	0.012	0.009
$\Delta(\partial\sigma/\partial x')$	< 0.001	0.006
$\Delta(\partial\sigma/\partial y')$	0.012	0.003
$\Delta(\partial\sigma/\partial E)$	0.031	0.018
ΔA_I	0.008	0.008
ΔGain	0.034	0.016
ΔTails	0.145	0.034
ΔInversion	0.026	0.074
ΔAnalysis	0.029	0.611
ΔP	0.109	0.117
Total systematic error	0.192	0.628
Statistical error	2.416	4.331

varying the respective correction factors independently by $\pm 25\%$, and the resulting change in A_n was taken as a conservative estimate of sensitivity to imperfect beam corrections.

The contribution from residual beam-current asymmetry (ΔA_I) was estimated by adding the statistical error of its mean to the systematic budget. Fluctuations of the PMT signal offsets (ΔGain) were assessed using all calibration runs: the offsets were varied within one standard deviation, and the accumulated effect was divided by $\sqrt{N_{calib}}$ to account for statistical fluctuations. Possible nonlinearities in the asymmetry correction (ΔTails) were estimated by excluding the 0.1% of events with the largest absolute corrections for each term in the asymmetry equation, summing the resulting shifts in the mean asymmetry.

To test for possible instrumental asymmetries from the polarity control system, a half-wave plate in the optical system at the beam source [21] was used to reverse the beam polarization independently of the electronics. A similar number of events was collected for both half-wave plate states (GVZ in and GVZ out in Fig. 2). Although the observed difference in A_n was not statistically significant, the estimated change for an equal number of events in
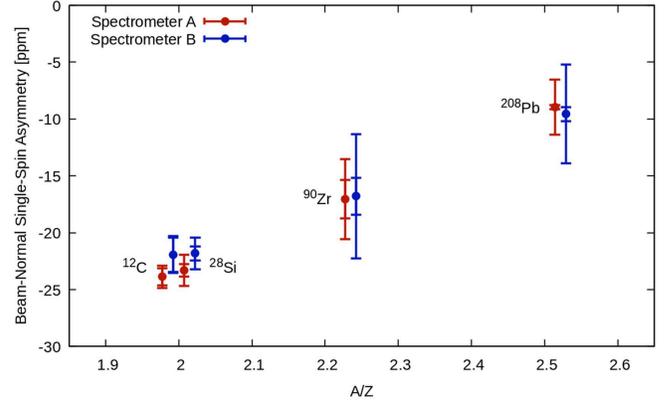

FIG. 3. Comparison of the beam-normal single-spin asymmetries of all nuclei measured at MAMI with similar kinematics plotted versus the atomic number over nuclear charge ratio. For better visibility, data points with identical ratios are shifted apart. The data points on the bottom left correspond to ^{12}C and ^{28}Si, the central point represents ^{90}Zr. The new data points for ^{208}Pb are shown on the top right.

both states was conservatively added as an additional uncertainty (ΔInversion). The small spread between the almost identical results of the two independent analysis chains was conservatively included as ΔAnalysis. The uncertainty of the beam polarization (ΔP) was added separately. All contributions were summed in quadrature to obtain the total systematic uncertainty.

Our new measurement yields a beam-normal single-spin asymmetry of $A_n = -9.1 \pm 2.1_{stat} \pm 0.7_{syst}$ ppm at a beam energy of 570 MeV and $Q^2 = 0.04$ GeV$^2/c^2$. This value is significantly different from zero and contrasts with the vanishing asymmetry reported by PREX Collaboration at 1.06 GeV [11]. This suggests a non-negligible energy dependence of TPE effects not captured by current theoretical models. A comparison across all measured nuclei at MAMI indicates a general decrease in $|A_n|$ with the mass-to-charge ratio A/Z, as visualized in Fig. 3. Within the present uncertainties, the apparent difference—most notably between ^{12}C and ^{28}Si on one side and ^{208}Pb on the other—may hint at indirect nuclear-structure effects, such as neutron skins or inelastic contributions. The observed A/Z trend appears to depend on kinematics: at higher beam energies, as in the CREX measurement [12], $|A_n|$ remains nearly constant up to $A/Z \approx 2.4$ and then drops sharply for ^{208}Pb. This indicates that no single empirical parametrization can capture the behavior across all energy regimes.

Updated calculations include new Compton form factors and Coulomb distortions by incorporating inelastic intermediate-state contributions as an absorptive optical potential in the Dirac equation [22]. Within this approach, the electron-nucleus interaction is represented by a real Coulomb term, accounting for elastic intermediate states,

and an imaginary term derived from the total photoabsorption cross section of the nucleus, which effectively describes inelastic processes. This formalism goes beyond earlier plane-wave treatments by consistently solving the relativistic Dirac equation with both potentials and by including subleading logarithmic contributions. These refinements lead to a significantly improved description of light and intermediate nuclei (^{4}He, ^{12}C, ^{27}Al, ^{48}Ca) at GeV energies but still fail to reproduce the PREX [11] and PREX-II [12] measurement on ^{208}Pb. The persistence of this discrepancy, despite the inclusion of Coulomb distortions and inelastic effects, suggests that present models miss an additional Z-dependent mechanism.

Moreover, the same theoretical framework that performs well at higher energies fails to describe the larger asymmetries observed at lower energies at MAMI, indicating that further refinements—possibly involving multiphoton exchange or explicit low-energy nuclear excitations—are required. At present, no self-consistent theoretical description simultaneously accounts for the combined energy and mass dependence of A_n across all kinematic regimes. Interestingly, simplified estimates [23] based on the same phenomenological Compton inputs but retaining only the leading logarithmic term reproduce the new MAMI result for ^{208}Pb reasonably well. However, these calculations omit Coulomb distortions and subleading contributions [10] and therefore cannot be regarded as a consistent theoretical explanation.

Ongoing efforts, including a proposal at the Thomas Jefferson National Accelerator Facility [24], aim to systematically test the nuclear dependence of TPE-related radiative corrections. These discrepancies and open questions reinforce the importance of a systematic study of A_n across a range of beam energies and nuclear targets. In particular, for the planned Mainz radius experiment (MREX), which aims to determine the neutron skin of ^{208}Pb at 155 MeV using parity-violating electron scattering, a reliable understanding of A_n is essential, as it may become a dominant source of systematic uncertainty. To address this, a new measurement campaign on lead is planned at MAMI, and future opportunities at the MESA accelerator at lower energies will further constrain the role of TPE in heavy nuclei.

Data availability—The data that support the findings of this article are not publicly available upon publication because it is not technically feasible and/or the cost of preparing, depositing, and hosting the data would be prohibitive within the terms of this research project. The data are available from the authors upon reasonable request.

[1] A. Sirlin, Phys. Rev. D **22**, 971 (1980).
[2] C. E. Carlson and M. Vanderhaeghen, Annu. Rev. Nucl. Part. Sci. **57**, 171 (2007).
[3] P. G. Blunden, W. Melnitchouk, and J. A. Tjon, Phys. Rev. Lett. **91**, 142304 (2003).
[4] M. Gorchtein and C. J. Horowitz, Phys. Rev. Lett. **102**, 091806 (2009).
[5] R. Pohl, A. Antognini, and F. Nez, Annu. Rev. Nucl. Part. Sci. **63**, 175 (2013).
[6] A. De Rújula, J. Kaplan, and E. de Rafael, Nucl. Phys. **B35**, 365 (1971).
[7] B. Pasquini and M. Vanderhaeghen, Eur. Phys. J. A **24**, 29 (2005).
[8] A. Afanasev and N. P. Merenkov, Phys. Rev. D **70**, 073002 (2004).
[9] E. D. Cooper and C. J. Horowitz, Phys. Rev. C **72**, 034602 (2005).
[10] M. Gorchtein and C. J. Horowitz, Phys. Rev. C **77**, 044606 (2008).
[11] S. Abrahamyan *et al.*, Phys. Rev. Lett. **109**, 192501 (2012).
[12] D. Adhikari *et al.*, Phys. Rev. Lett. **128**, 142501 (2022).
[13] K. Blomqvist *et al.*, Nucl. Instrum. Methods Phys. Res., Sect. A **403**, 263 (1998).
[14] A. Jankowiak, Eur. Phys. J. A **28**, 149 (2006).
[15] A. Esser *et al.*, Phys. Rev. Lett. **121**, 022503 (2018).
[16] A. Esser *et al.*, Phys. Lett. B **808**, 135664 (2020).
[17] A. Esser *et al.*, Nucl. Instrum. Methods Phys. Res., Sect. A **1072**, 170187 (2025).
[18] N. G. de Bruijn, Nederl. Akad. Wetensch. **49**, 758 (1946), https://pure.tue.nl/ws/files/4442708/597473.pdf.
[19] F. Anghinolfi, P. Jarron, A. N. Martemiyanov, E. Usenko, H. Wenninger, M. C. S. Williams, and A. Zichichi, Nucl. Instrum. Methods Phys. Res., Sect. A **533**, 183 (2004).
[20] B. Schlimme *et al.*, Nucl. Instrum. Methods Phys. Res., Sect. A **850**, 54 (2017).
[21] K. Aulenbacher, Eur. Phys. J. A **32**, 543 (2007).
[22] O. Koshchii, M. Gorchtein, X. Roca-Maza, and H. Spiesberger, Phys. Rev. C **103**, 064316 (2021).
[23] M. Gorchtein (private communication).
[24] C. Gal *et al.*, arXiv:2411.10267.